공학석사 학위논문

A study of the Nonlinear Piezoelectric ZnO Dual Sensor for the Detection of Bending Angle and Radius

2017년 8월

서울대학교 대학원

융합과학부 나노융합전공

이 화 진

A study of the nonlinear piezoelectric ZnO Dual Sensor for the Detection of Bending Angle and Radius

지도 교수 김연상

이 논문을 공학석사 학위논문으로 제출함
2017년 5월

서울대학교 대학원

융합과학부 나노융합전공

이 화 진

이화진의 석사 학위논문을 인준함
2017년 5월

위 원 장 박 원 철 (인)

부위원장 김 연 상 (인)

위 원 이 태 일 (인)

Abstract

A study of the nonlinear piezoelectric ZnO Dual Sensor for the Detection of Bending Angle and Radius

Hwa-jin Lee

Program in Nano Science and Technology

The Graduate School of

Seoul National University

A non-linear piezoelectric dual sensor consisting of one-directionally and randomly aligned bi-axially grown zinc oxide nanorods was introduced for simultaneous detection of the bending radius and angle of a bending

deformation. The tendency of the voltage peak according to the bending radius and angle was experimentally measured and theoretically calculated using COMSOL Multiphysics®. For the sensing measurements, the bending radius was set as the independent variable, and both the average voltage peak and the rate of change of the voltage peak value with respect to the bending angle were set as dependent variables. Based on these variables, an algorithm is designed to simultaneously recognize the bending radius and angle. Finally, a two-channel nonlinear piezoelectric dual sensor was fabricated and the bending radius and angle were successfully identified through the proposed algorithm with various bending deformations.

Keywords: Self-powered sensor, BG-ZnO NR, nonlinear piezoelectricity, sensing algorithm, bending radius, bending angle

Student Number: 2015-26093

Table of Contents

List of Figures and Tables

Spray-coating of the flexible Ag NW-SWCNT electrode. 4) Integrating randomly and one-directionally aligned devices on both sides of the PC substrate.

Figure 7. The SEM image of the morphology of the top electrode, Ag NW-SWCNT.

Figure 8. (a) SEM image of a single crystalline BG-ZnO NR and (b) one-directionally and (c) randomly aligned monolayer formed by rubbing process. (d) Changes of total light intensity incident into eyepiece by rotating the monolayer film under the cross-polarized light illumination and optical image of each case was presented. All the scale bar was $100\ \mu m$, respectively.

Figure 9. The large area of SEM images rubbing in (a) one-directionally and (b) randomly. The respective six zone's scale bars represent 10 μm.

Figure 10. (a) The standard open-circuit voltage signals of randomly aligned BG-ZnO NRs. Average voltage peaks of randomly aligned monolayer with different bending angle of (b) convexly and (c) concavely bent case. (d) The standard open-circuit voltage signals of one-directionally BG-ZnO NRs. The average voltage peaks of one-directionally aligned

monolayer with different bending angle of (e) convexly and (f) concavely bent case.

Figure 11. Deformation of a BG-ZnO NR with a displacement vector = (0, $r - \sqrt{r^2 - z^2}$, 0) and the rotation of a BG-ZnO NR (rotation center = y-axis).

Figure 12. (a) Calculated distribution of the nonlinear piezoelectric potential in a BG-ZnO NR, lying in the plane direction of the bent substrate at 0.03 m bending radius with different bending angles from 0° to 90°. Calculated average voltage difference along the y-axis under a given bending angle (b) and bending radius (c).

Figure 13. Measured average voltage peaks and slope of voltage peak versus bending angle with respect to bending radius, and their linearly fitted values for (a) randomly and (b) one-directionally aligned BG-ZnO NRs.

Figure 14. The experimentally fitted equations from **Figure 12**.

Figure 15. (a) Schematic diagram of nonlinear piezoelectric dual sensors (b) output voltage peaks from two channels under the three types of bending deformation.

Chapter 1. Introduction

1.1 Bending detection technology

In accordance with demands of electronic bending sensors to detect free and smooth movement of a living body for the 'internet of things' (IoT) technology (**Figure 1**), electronic bending sensor have been actively studied [1-4]. Bending detection is a key technology that needs to be developed in areas such as artificial skin [5-6], soft robotics [7], human motion detection [8] etc (**Figure 2**).

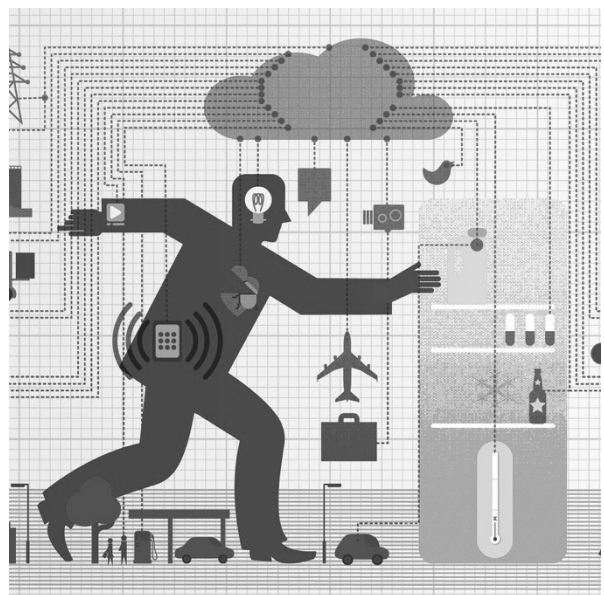

Figure 1. Schematic graphic image of representing the Internet of things (IoT) technology (from © 1996-2017 McKinsey & Company).

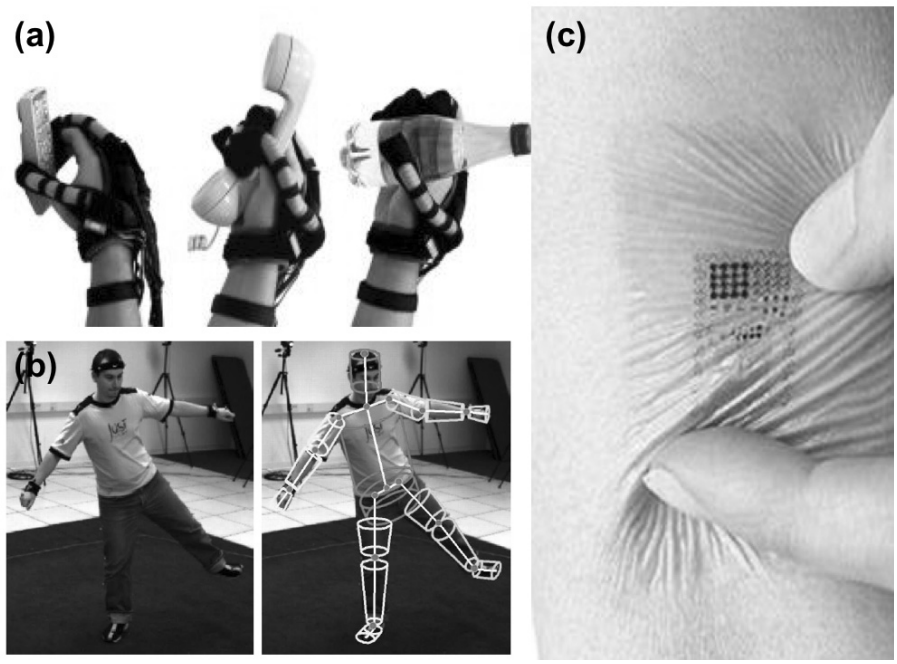

Figure 2. Needs for bending detection technology in industry, (a) robotic hands (from © 2017 THE IRISH TIMES), (b) human motion detection (from Brown University Computer Science) , (c) artificial skin (from photo courtesy of MC10).

1.2 Recent research of Bending sensor

To date, many concepts based on various physical principles have been introduced for electronic devices that recognize bending [9-11]. Among them, the piezoelectric principle is the most likely to be commercialized, which provides a simple configuration and is capable of active sensing. Recently, many reports of bending sensors based on piezoelectric materials have surfaced. For example, the polyvinylidene fluoride (PVDF) [12], hybrid ZnO / PVDF [13-14], cellulose nanofibrils (CNF),[15] CNF/ polydimethylsiloxane (PDMS) aerogel [16] and tellurium nanofiber [17] etc.

1.3 Nonlinear piezoelectricity

Essentially, bending is a nonlinear deformation; however, most piezoelectric bending sensors have adopted the linear piezoelectric, d_{33} or d_{31} mode (**Figure 3**), which uses vertical or parallel electrical polarization to the given deformation because the direction of piezoelectric polarization can be in-plane or out-of-plane. The electrode configuration was preferred to be out-of-plane based on the degree of integration and the process convenience of the sensor [18]. It is necessary to develop a sensor based on the nonlinear piezoelectric mode that is suitable for the nonlinear deformation of bending. In addition, the electrical signal generated from the linear piezoelectric bending sensor has been interpreted based on the relationship between the signal intensity and the magnitude of the bending radius [19-21]. However, in order to advance the bending sensor technology, it is necessary to develop a sensor capable of describing various features of bending deformation such as bending angle, bending radius, bending speed, etc.

In this study, we introduced one-directionally aligned bi-axially grown (BG) ZnO nanorods (NRs), which could simultaneously identify bending radius and bending angle, and demonstrate the performance of the bending sensor fabricated using both of these properties. Unlike the conventional piezoelectric material, BG-ZnO NR was activated under the out-of-plane

electrode configuration through μ_{31} mode (**Figure 4**). This working mechanism was related with equation $\Delta\vec{p} = \overrightarrow{p_f} - \overrightarrow{p_i}$. For Figure 4a, each of two ZnO NR generated upper potential resulting as polarization. The relating μ_{ij} is flexoelectric coefficient, a second rank polar tensor which of μ_{31} mode represents that lateral force applied in the direction is perpendicular to the polarization direction. Basically, the flexoelectricity was generated when apply of an elastic strain gradient resulting electric polarization in an insulating solid which specialized in nonlinear piezoelectricity. In contrast with BG-ZnO NR, uni-axially grown ZnO shown sum zero potential as it shown in Figure 4b throughout the bending deformation. The μ_{31} mode of BG-ZnO NR is adjustable for bending deformation [22], while its one-dimensional shape provides sensitive piezoelectric behavior to the bending angle. These piezoelectric properties were experimentally demonstrated and the corresponding mechanisms were confirmed by theoretical calculation using COMSOL Multiphysics®. Finally, we fabricated a device that simultaneously recognizes the bending radius and bending angle, which successfully illustrated the sensing performance by analyzing the electrical signals generated under various bending deformations.

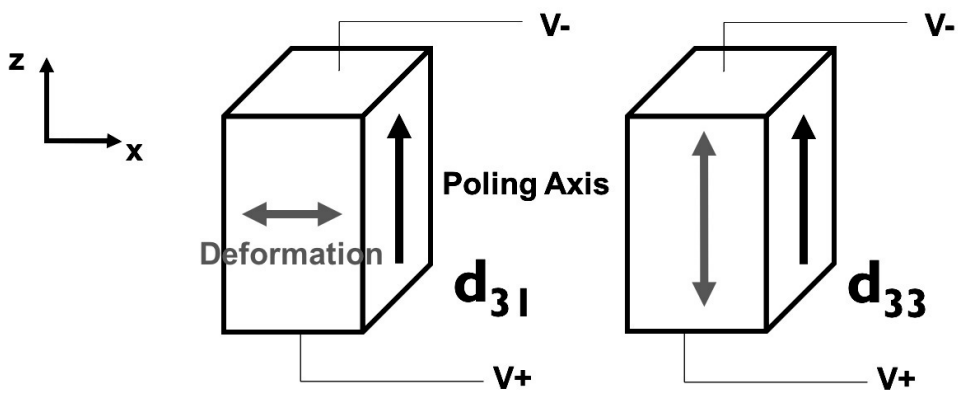

Figure 3. The concept illustration of d_{31} and d_{33} mode.

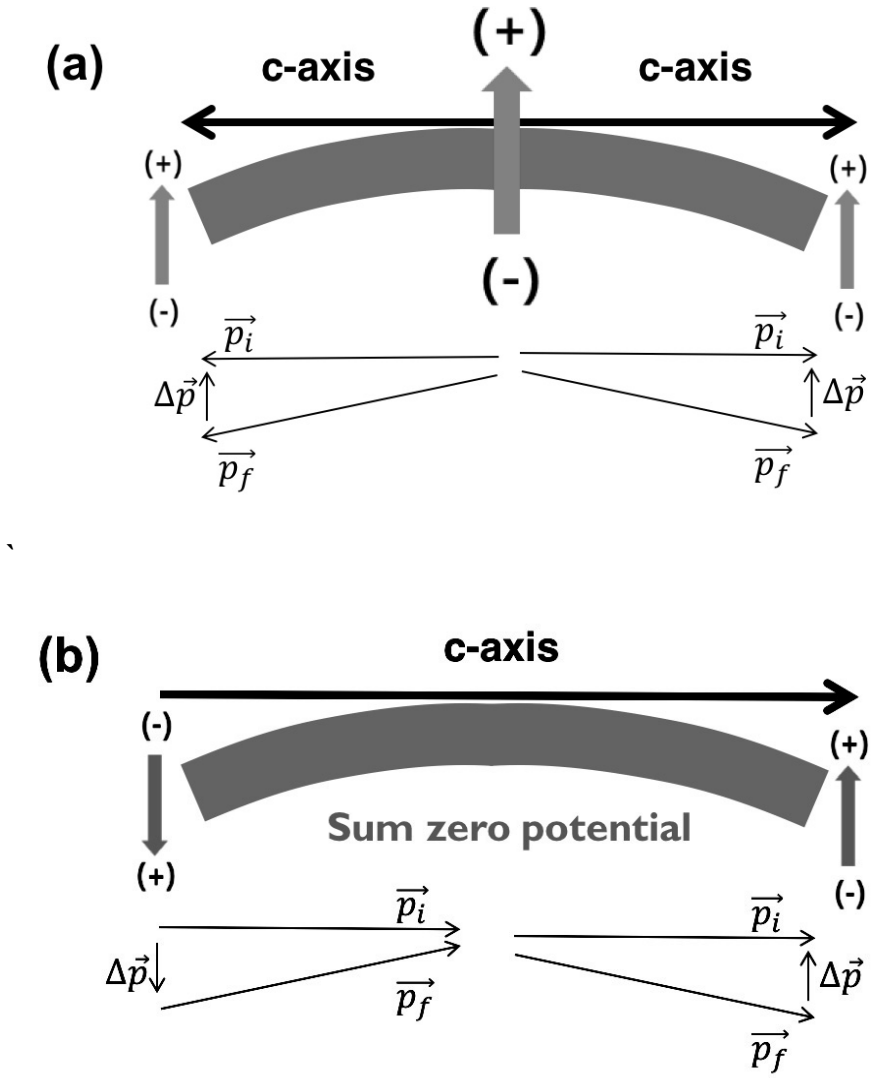

Figure 4. The working mechanism of (a) bi-axially grown zinc oxide nanorods, (b) uni-axially grown zinc oxide nanorods.

Chapter 2. Experimental details

2.1 Synthesis of bi-axially grown ZnO nanorods

To synthesize BG-ZnO NRs, the reagents: zinc nitrate hexahydrate ($Zn(NO_3)_2 \cdot 6H_2O$) [Sigma Aldrich, ≥ 99.0 %] and hexamethylenetetramine (HMTA) ($C_6H_{12}N_4$) [Sigma Aldrich, ≥ 99.0 %], were used and formatted through wet chemical methods to kinetically control the uniform shape of BG-ZnO NRs [26]. Each of the solutes was dissolved into a 120 ml deionized water (D.I water), with an amount of 0.178 g $Zn(NO_3)_2 \cdot 6H_2O$ and 80 ml D.I water of HMTA 0.056 g as the mol ratio of 6:4. First, the solution of HMTA was dissolved under magnetic stirring at 500 rpm in 250 ml round flask and heated constantly with predesigned heating block at 80 °C. Second, droplets of the $Zn(NO_3)_2 \cdot 6H_2O$ solution were added consecutively by using a syringe pump [NE-1000] with an injection rate of 2 ml/min and a reaction time of 30 min. The overall synthesized BG-ZnO NRs were purified by vacuum filtration using a membrane filter with a 0.2 μm pore size [Macherey-Nagel, Porafil-CA], which was dispersed with ethanol and dried in an 80 °C hot plate for 1 h, resulting in an off-white powder. The entire process of synthesizing was schemed in **Figure 5**.

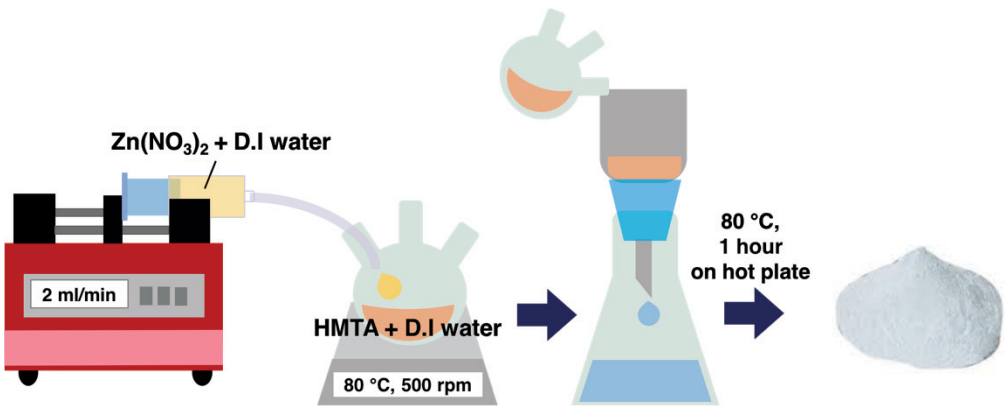

Figure 5. The schematic illustration of synthesizing BG-ZnO NRs.

2.2 Fabrication of nonlinear piezoelectric dual sensor

The fabrication for the nonlinear piezoelectric dual sensor fabrication was shown in **Figure 6**. First, the ITO-PET (indium tin oxide on the polyethylene terephthalate) [Sigma Aldrich, $60\ \Omega/sq$] substrate of ITO (indium tin oxide) was formed as the bottom electrode by using an etching process with hydrochloric acid (HCl). The etching process conducted for 15 min with HCl [DAEJUNG, ≥ 35 %] and spin coated for 30 s, 2500 rpm with polydimethylsiloxane (PDMS) (PDMS : Hexane mixture in 5:5 weight ratio). The PDMS was spin coated on the ITO-PET and annealed at 80 °C for 30 min. The synthesized BG-ZnO NRs were rubbed on the PDMS coated ITO-PET using a paint brush in a unidirectional and random alignment. The PDMS was spin coated again on the substrate and cured at 80 ℃ on the hot plate. Before defining the top electrodes, the oxygen (O_2) Plasma [FEMTO SCIENCE CUTE] treatment with 100 W, in 5 min was used to treat the surface of the second PDMS-coated film to make it hydrophilic.

Before depositing the top electrodes, the surface of the second PDMS layer was treated to be hydrophilic by using O_2 plasma. The top electrode was defined by using of spray coating method using a mixture of two reagents: silver nanowire-single walled carbon nanotube (AgNW-SWCNT)

[Nanopyxis, 1 wt% in distilled water] and SWCNT [Nano Solution Co. Ltd. 1.3 wt% in distilled water stabilized by sodium dodecyl sulfonate (SDS) surfactants] (7:3) (g:g) with a predesigned shadow mask. The spray coating method was conducted using the hand-made acryl box with a spray nozzle on the top of the box and was connected to a syringe pump to deposit the top electrodes. The continuous blowing of the 6 bar, 5 L/min N_2 gas was agitated during the solution injection with a syringe pump at a rate of 0.2 ml/min, which was simultaneously annealed on a hot plate at 100 °C. The Ag NW-SWCNT spray-coated device was then washed with D.I water to remove the remaining SDS surfactants. As shown in the last schematic diagram in **Figure 6**, the whole device was completed by fixing the sensing units, consisting of a one-directionally and randomly aligned monolayer of BG-ZnO NRs, on both sides of the polycarbonate (PC), respectively. Each sensing unit independently generates electrical signals, which are combined and interpreted for simultaneously detecting the bending radius and bending angle of the PC substrate. In all cases, the thickness of substrate, PC (1 mm) was same.

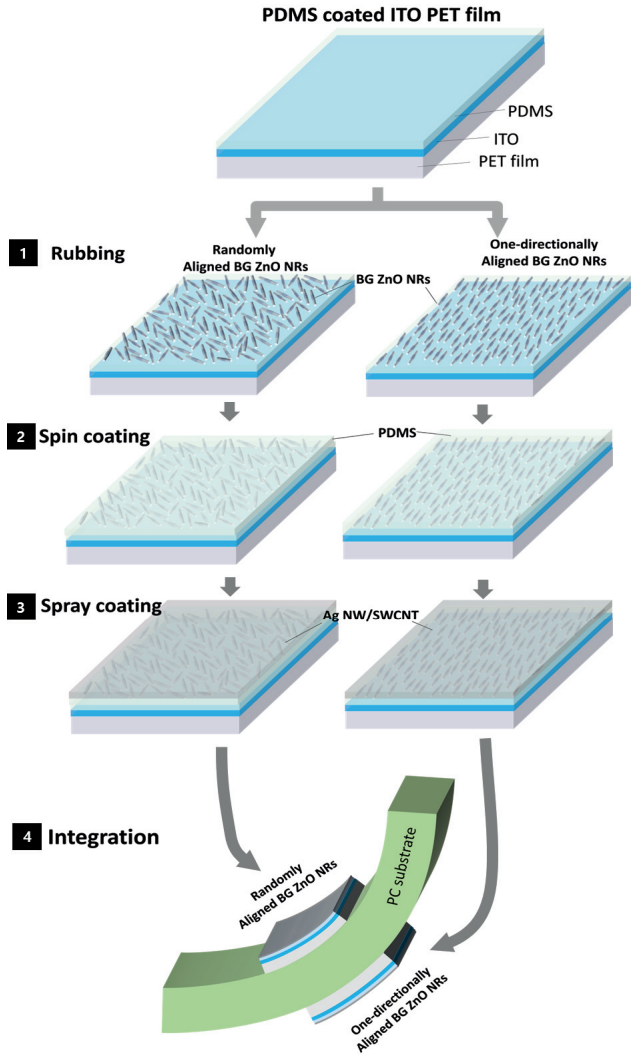

Figure 6. Schematic illustration describing a process for the fabrication of a non-linear piezoelectric dual sensors sensor. 1) Rubbing one-directionally and randomly aligned BG-ZnO NRs onto PDMS coated ITO-PET films. 2) Spin coating with diluted PDMS solution and annealing on a hot plate. 3) Spray-coating of the flexible Ag NW-SWCNT electrode. 4) Integrating randomly and one-directionally aligned devices on both sides of the PC substrate.

2.3 Characteristics of nonlinear piezoelectric dual sensor

The morphology of BG-ZnO NRs and the hybrid Ag NW-SWCNT were investigated through the field-emission scanning electron microscope (FE-SEM) [Hitachi S-4800]. The morphology of the top electrode of Ag NW-SWCNT was shown in **Figure 7**. The orientation of the rubbing BG-ZnO NRs were proved over POM [BX60F5]. The overall images were observed on a CCD camera (KON3.1) mounted on the optical microscope. The photographs were digitized by a video frame grabber with a resolution of 2048 (horizontal) by 1536 (vertical) pixels and analyzed using the Photoshop software for the selection, recognition, and separation of colors. A selected area on the monitor depicts the RGB or luminosity of digitized images including the median and standard deviation. The percentage of intensities (I/I_0) was measured through the Photoshop-based luminosity integral of imported images. The electrical output, especially open-circuit voltages of our sensor were recorded using an oscilloscope [Tektronix MDO 3024] with each of input impedance and capacitance 10 MΩ and 3.9 pF, while the constant speed of the bending motion was performed by a mechanical bending machine [Z-tec].

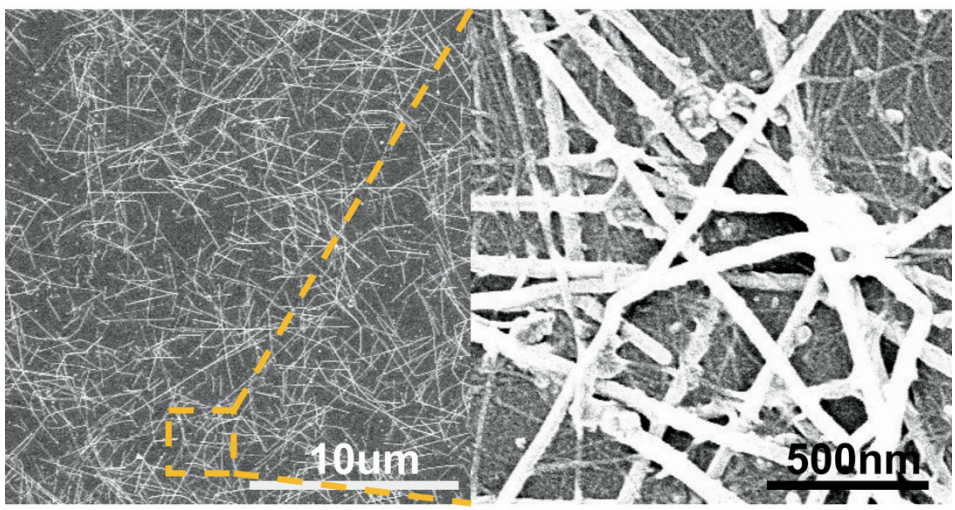

Figure 7. The SEM image of the morphology of the top electrode, Ag NW-SWCNT.

Chapter 3. Results and Discussion

3.1 Investigation of the monolayer of bi-axially grown ZnO NRs

To investigate the monolayers consisting of one-directionally and randomly aligned BG-ZnO NRs, we evaluated the degree of alignment through scanning electron microscopy (SEM) and polarized light optical microscopy (POM). The shape of a BG-ZnO NR was shown in **Figure 8a**, which of its length and width were about 2.5 μm and 300 nm, respectively. It was clearly observed that ZnO crystal grows on both sides of the c-axis centering on the intermediate plane. This crystallographic shape was an important property that provides nonlinear piezoelectricity.

As shown in **Figure 8b-c**, each of one-directional and random aligned monolayer was formed by rubbing process with a powder of the BG-ZnO NRs. To evaluate the degree of alignment for each monolayer, we conducted the statistical calculation where the angle between the longitudinal direction of each NR and a rubbing direction counted as the degree of alignment of one-directionally rubbed case was 92.561($\pm$ 6.57) % aligned, while randomly rubbed case was 58.901($\pm$37.48) %. The counted values were come from average and their standard deviations. The additional observations on the alignment in a large area are shown in **Figure 9**.

To confirm the degree of alignment for the one-directionally rubbed monolayer over the large area, we performed a POM analysis as shown in **Figure 8d**. After setting the cross-pole of the POM, the rubbed BG-ZnO NR samples were placed on the object holder, and the ratio of the light intensity of the lower light source to the contact lens was evaluated while rotating the object holder from 0° to 180°. As shown in **Figure 8d**, 45% of light leakage was observed in the cross-pole condition for all rotational angles for the randomly rubbed sample. Additionally, the light leakage periodicity according to rotation angle with two minimum values of 40% at 0° to 180° and a maximum value of 67% at 90° for one-directionally rubbed samples was observed. In the case of random rubbing, the uniform light leakage due to scattering by each BG-ZnO NR was generated, regardless of the rotation angle of the object holder. In the case of the one-directional rubbing, periodic light leakage with the rotation angle was observed according to the polarization characteristics of aligned BG-ZnO NRs. The optical image below **Figure 8d** show the appearance of light leakage according to the rotation angle.

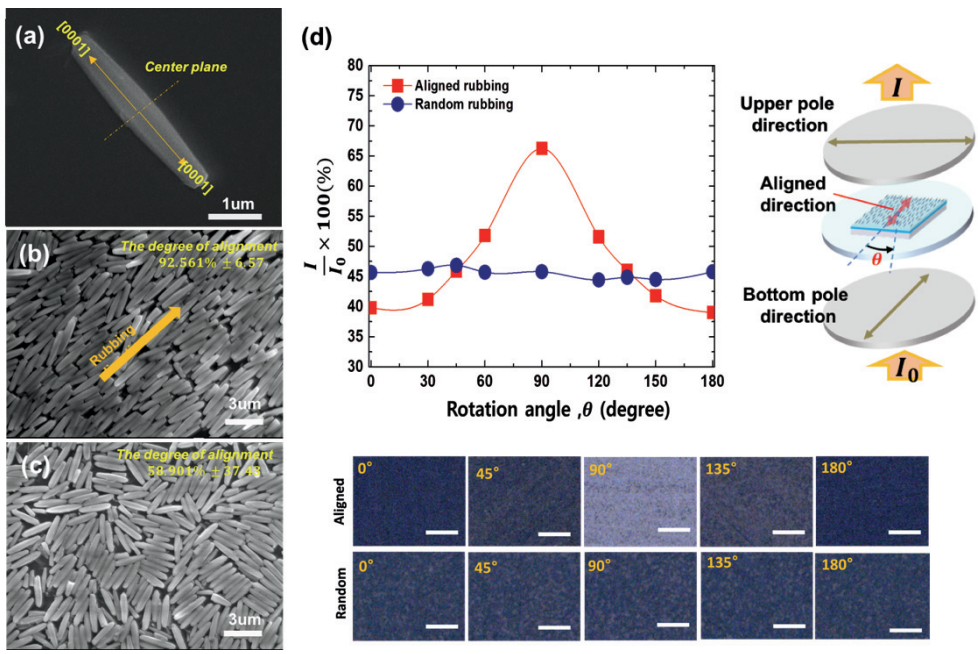

Figure 8. (a) SEM image of a single crystalline BG-ZnO NR and (b) one-directionally and (c) randomly aligned monolayer formed by rubbing process. (d) Changes of total light intensity incident into eyepiece by rotating the monolayer film under the cross-polarized light illumination and optical image of each case was presented. All the scale bar was $100\,\mu m$, respectively.

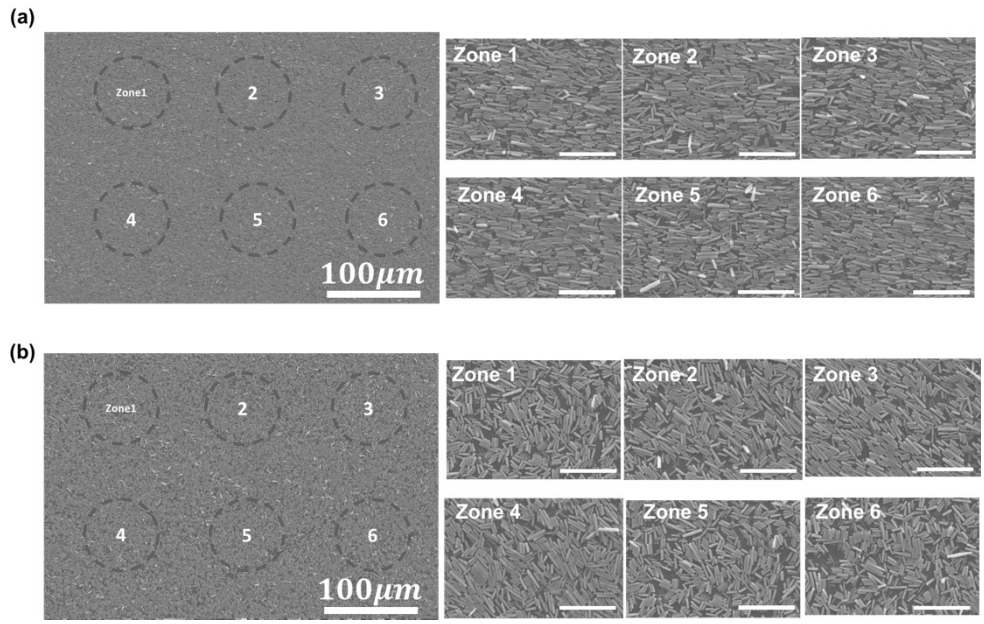

Figure 9. The large area of SEM images rubbing in (a) one-directionally and (b) randomly. The respective six zone's scale bars represent 10 μm.

3.2 Output performance of nonlinear piezoelectric dual sensor

A typical voltage signal from randomly aligned BG-ZnO NRs under the concave bending with constant bending speed (150 mm/sec) and several values of bending radii (55 mm, 50 mm, 43 mm, 36 mm, 31 mm) were displayed in **Figure 10a**. It was observed that the peak value of the signal increases as the bending radius increases. When we concavely bend the randomly aligned BG-ZnO NRs with a different bending angle as shown in Fig. 3b, the magnitude of the voltage was constant regardless of the bending angle (0°, 22.5°, 45°, 67.5°, 90°). This tendency was also confirmed in the case of the convex bending as shown in **Figure 10c**. However, the size of the voltage peak of the convex bending was slightly larger than that of the concave bending at the same bending radius.

On the other hand, in the case of the one-directionally aligned BG-ZnO NRs, the shape and magnitude of the voltage peak were similar to that of the randomly aligned BG-ZnO NRs with respect to the bending radius as shown in **Figure 10d**. However, a clear change in the voltage magnitude of the bending angle was observed in this case. In **Figure 10e**, as the bending angle increased from 0° to 90°, the voltage tended to decrease linearly. This result was believed to be due to the correlation between the aligned direction of BG-ZnO NR and the bending angle. As shown in **Figure 10f**, it was

confirmed that there was a change in the voltage according to the bending angle for the convex bending. All measured values in **Figure 10** were captured in **Table 1 to 4** with their standard deviations.

The voltage origin of the device was explained through fundamental piezoelectric theory, on how BG-ZnO NR has its own intrinsic piezoelectric potential, which was proportional to the tensile strain but independent of the longitudinal direction [23]. In addition, the whole fabricated device was bent with nonlinear deformation, which activated under nonlinear piezoelectricity μ_{31} mode [24], so our working device was driven under the equation, $P_i = e_{ijk}\varepsilon_{jk} + \mu_{ijkl}\varepsilon_{jk,l}$, where, P_i is the polarization vector, e is the matrix of piezoelectric coefficient, ε is the matrix of strain tensor, and μ is the flexoelectric tensor. However, as BG-ZnO NR had a structure in which the c-axis is aligned with each other with respect to the center plane, the potentials due to the linear piezoelectric constant inevitably cancels each other. Therefore, the main polarization change of BG-ZnO NR through bending was contributed by a non-linear piezoelectric term [25].

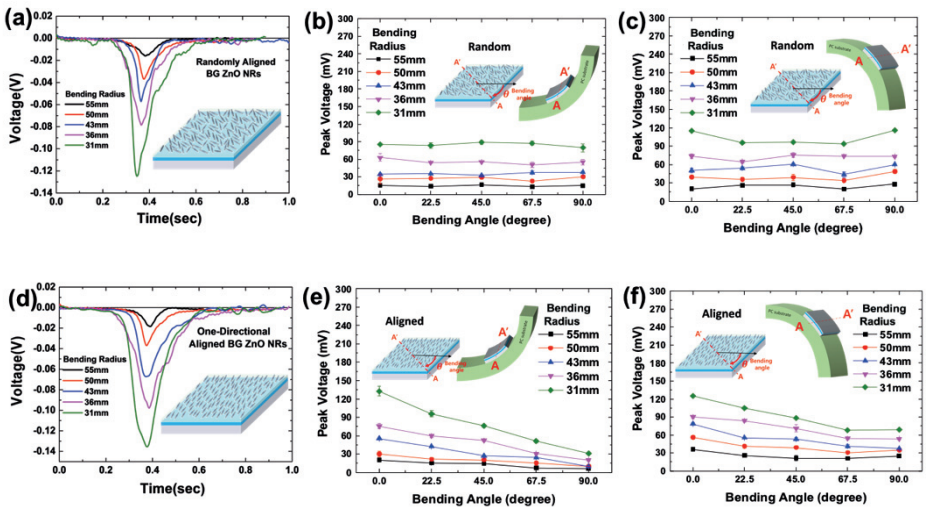

Figure 10. (a) The standard open-circuit voltage signals of randomly aligned BG-ZnO NRs. Average voltage peaks of randomly aligned monolayer with different bending angle of (b) convexly and (c) concavely bent case. (d) The standard open-circuit voltage signals of one-directionally BG-ZnO NRs. The average voltage peaks of one-directionally aligned monolayer with different bending angle of (e) convexly and (f) concavely bent case.

Bending Radius (mm) / Bending Angle(°)	55	50	43	36	31
90	15.5 (±3)mV	26.15 (±8.13)mV	34.333 (±2.0207)mV	63 (±6.555)mV	85.83 (±1.255)mV
67.5	13.66667 (±0.577)mV	27.16665 (±2.0205)mV	35.333 (±1.607)mV	54 (±0.5)mV	84 (±4.4814)mV
45	16.5 (±0.5)mV	29 (±2.825)mV	32.66665 (±1.443)mV	55.75 (±1.765)mV	89 (±3.12)mV
22.5	13.1665 (±0.2885)mV	22.833 (±1.44335)mV	37.3333 (±2.75375)mV	50.83335 (±4.64575)mV	87.5 (±3.32915)mV
0	15.165 (±1.15)mV	29.83 (±0.76) mV	37.8333 (±1.5275)mV	55.165 (±4.725)mV	79.83 (±6.895)mV

Table 1. The measured voltage peaks under the convex bending for the randomly aligned BG-ZnO NRs.

Bending Curvature (mm) / Bending Angle(°)	55	50	43	36	31
90	20.33 (±1.525) mV	30 (±4.365) mV	55.33 (±0.76) mV	75.665 (±4.25) mV	133 (±7.6) mV
67.5	15.33 (±0.76) mV	21.33 (±1.04) mV	42.33 (±0.76) mV	59.83 (±2.84) mV	95.83 (±4.98) mV
45	14.5 (±2.595) mV	20.25 (±2.47) mV	27 (±1) mV	52.165 (±1.255) mV	75.83 (±2.02) mV
22.5	7.33 (±0.2885) mV	15.165 (±1.04) mV	24.665 (±1.255) mV	30.665 (±1.04) mV	51 (±2.29) mV
0	6.525 (±0.035) mV	10 (±0.408) mV	9.33 (±1.04) mV	20.33 (±1.04) mV	30.665 (±0.285) mV

Table 2. The measured voltage peaks under the concave bending for the randomly aligned BG-ZnO NRs.

Bending Radius (mm) / Bending Angle(°)	55	50	43	36	31
90	20.33 (±1.525)mV	30 (±4.365)mV	55.33 (±0.76)mV	75.665 (±4.25)mV	133 (±7.6)mV
67.5	15.33 (±0.76)mV	21.33 (±1.04)mV	42.33 (±0.76)mV	59.83 (±2.84)mV	95.83 (±4.98)mV
45	14.5 (±2.595)mV	20.25 (±2.47)mV	27 (±1)mV	52.165 (±1.255)mV	75.83 (±2.02)mV
22.5	7.33 (±0.2885)mV	15.165 (±1.04)mV	24.665 (±1.255)mV	30.665 (±1.04)mV	51 (±2.29)mV
0	6.525 (±0.035)mV	10 (±0.408)mV	9.33 (±1.04)mV	20.33 (±1.04)mV	30.665 (±0.285)mV

Table 3. The measured voltage peaks under the convex bending for the one-directionally aligned BG-ZnO NRs

.

Bending Angle(°) \ Bending Radius (mm)	55	50	43	36	31
90	36.165 (±2.75)mV	55.665 (±2.925)mV	78.5 (±2.29)mV	90 (±2.29)mV	125 (±5.655)mV
67.5	25.75 (±1.06)mV	40.83 (±2.152)mV	55.5 (±0.865)mV	83.5 (±2.12)mV	104.75 (±16.615)mV
45	21.25 (±3.887)mV	38.83 (±1.605)mV	53.165 (±2.515)mV	70.83 (±6.11)mV	88.33 (±1.755)mV
22.5	21 (±1.41)mV	30.5 (±1.8)mV	41.165 (±2.565)mV	54.165 (±2.305)mV	68 (±2.5)mV
0	24.665 (±1.525)mV	34.665 (±0.285)mV	37.165 (±0.285)mV	53.665 (±1.04)mV	68.75 (±3.885)mV

Table 4. The measured voltage peaks under the concave bending for the one-directionally aligned BG-ZnO NRs.

3.3 Theoretical investigation based on COMSOL Multiphysics®

To theoretically investigate the mechanism of the nonlinear piezoelectric potential change of BG-ZnO NR according to the bending angle, which was the main concern in this study, a computer simulation based on COMSOL Multiphysics® was carried out. The BG-ZnO NR used in the calculation was a symmetric wedge of 2.5 μm long with a hexagonal cross section and a diagonal line at the center of 500 nm and a value of 300 nm at the end. The crystal orientations of ZnO were set so that two crystals grown in the [0001] direction at the base of the center were turned back (**Figure 11**). The strain of BG-ZnO NR was applied by the given bending radius, and the bending angle was set by rotating the BG-ZnO NR at a similar bending radius. The nonlinear piezoelectric potentials of BG-ZnO NR were calculated as the difference between two surfaces obtained from the maximum values of the top and bottom surfaces.

As shown in **Figure 12**, a nonlinear piezoelectric potential of a single BG-ZnO NR lying in the plane direction of the substrate was calculated when the bending angle was modulated at a fixed bending radius of 0.03 m. Under the bending deformation, BG-ZnO NR generated a nonlinear piezoelectric potential in the direction perpendicular to the c-axis and this value tended to decrease as the bending angle changed from 0° to 90°.

For various other bending radius conditions, the nonlinear piezoelectric potentials were calculated and the results were shown in **Figure 12b**. As the bending angle becomes 90°, the potential difference between various bending radii tends to decrease because the bending deformation of BG-ZnO NR does not nearly occur at bending angle 90°. However, the theoretical tendency does not show a linearity, considering that the degree of alignment of BG-ZnO NR was not 100 % in the experiment. Because the effective bending angle of BG-ZnO NRs with respect to a bending angle set in the real device will have a certain range of values with a distribution related to the degree of alignment, the linear tendency of the nonlinear piezoelectric potential to set bending angles was considered observable in experimental measurement. Here, it should be noted that the experimental results of the decreasing tendency of the nonlinear piezoelectric potential with respect to the bending angle were in agreement with the theoretical results. The calculation result of the nonlinear piezoelectric potential with the bending radius under a given bending angle was shown in **Figure 12c**. As the bending radius increased, the nonlinear piezoelectric potential tended to decrease almost linearly. This result was also consistent with the experimental results as well as the tendency for the bending angle.

From the above experiments and calculations, it was clearly defined that for randomly aligned samples, the voltage signal depended only on the bending radius, while for one-directionally aligned samples, the voltage signal depended on the bending angle and radius. However, as the voltage signal of the one-directionally aligned sample was simultaneously dependent on the bending angle and radius, a sensing device and algorithm that could recognize both bending angle and radius from a bending deformation must be designed.

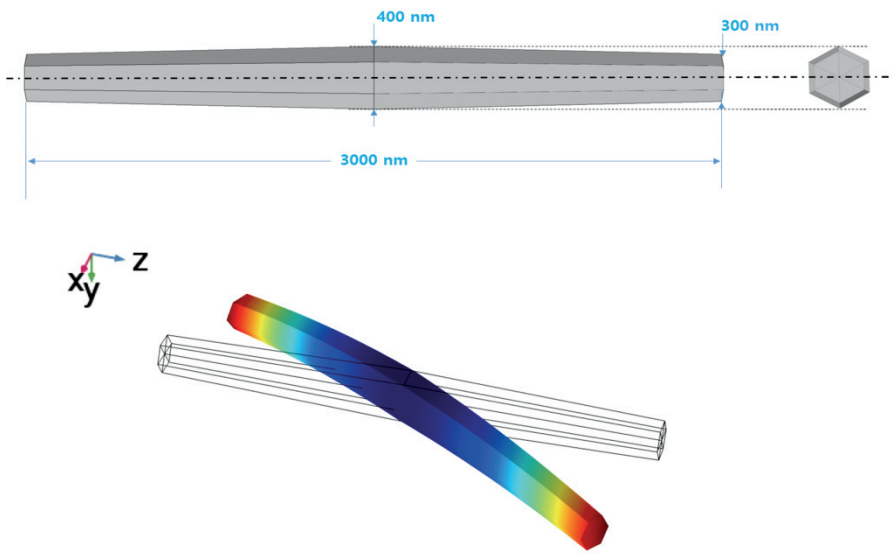

Figure 11. Deformation of a BG-ZnO NR with a displacement vector = (0, $r - \sqrt{r^2 - z^2}$, 0) and the rotation of a BG-ZnO NR (rotation center = y-axis).

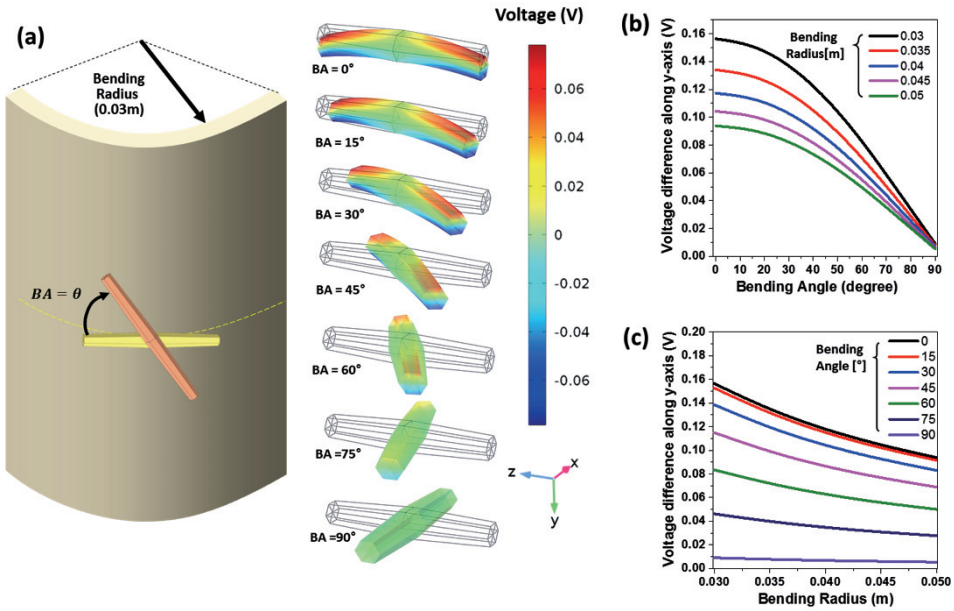

Figure 12. (a) Calculated distribution of the nonlinear piezoelectric potential in a BG-ZnO NR, lying in the plane direction of the bent substrate at 0.03 m bending radius with different bending angles from 0° to 90°. Calculated average voltage difference along the y-axis under a given bending angle (b) and bending radius (c).

3.4 Sensing algorithm based on experimental results

For this purpose, we introduced a new variable called the slope between voltage peak and bending angle as a dependent variable to recognize the bending angle, as the voltage signal generated from a bending deformation depended on both the bending radius and the angle. Therefore, we could consider two dependent variables of the slope and the peak voltage with respect to the bending radius value as an independent variable. In **Figure 13 a and b** show the results of summarizing the experimental values between the mentioned independent variable and dependent variables for randomly and one-directionally aligned samples. The fitted equations were shown in the **Figure 14** as a result of the specific linear fitting. It was possible to use these linear equations as an important record for simultaneously recognizing the bending angle and the radius as the main information of a bending deformation.

Based on the linear relationship between the abovementioned variables, the sensing algorithm proposed in this study assumes that a pair of randomly and one-directionally aligned samples should be located at a point on the substrate of a given bending deformation. These two samples were placed on the upper and lower surfaces of the substrate, respectively, so the situation of bending directions (convex or concave) opposite to each

other was considered. The diagram in **Figure 15a** illustrates this design. In our experiment, a randomly aligned sample was integrated on the concave surface as channel 2 and one-directionally aligned samples were integrated on the convex surface as channel 1.

In order for our algorithm to recognize the bending angle and radius simultaneously, the following steps were observed. In the first step, the voltage peak measured from channel 2 obtains information on the radius of deformation of the given bend from the fitted equation in **Figure 13a**. The second step was to find out the bending angle from the linear equation in **Figure 13b** from the voltage peak obtained from channel 1, based on the information of the as known bending radius. As a result, two sensors operated simultaneously for one bending deformation, to make it possible to detect the bending radius and angle information.

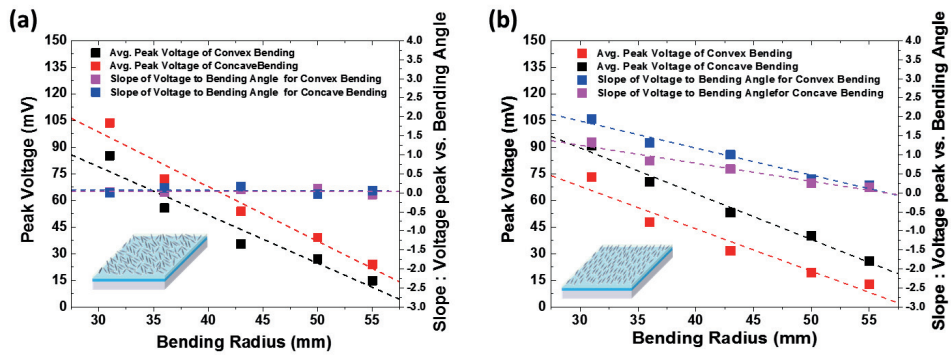

Figure 13. Measured average voltage peaks and slope of voltage peak versus bending angle with respect to bending radius, and their linearly fitted values for (a) randomly and (b) one-directionally aligned BG-ZnO NRs.

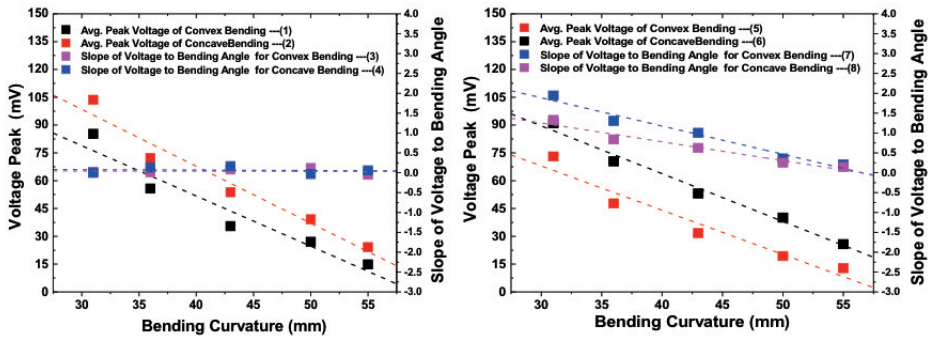

$$y = 160.23048 - 2.71105x \quad (1)$$

$$y = 190.55299 - 3.06929x \quad (2)$$

$$y = 0.11395 - 0.00116x \quad (3)$$

$$y = 0.05887 - 5.15568e^{-4}x \quad (4)$$

$$y = 166.88498 - 2.57704x \quad (5)$$

$$y = 139.57312 - 2.38707x \quad (6)$$

$$y = 4.019 - 0.07107x \quad (7)$$

$$y = 2.6732 - 0.04736x \quad (8)$$

Figure 14. The experimentally fitted equations from **Figure 13**.

3.5 Application of the fabricated nonlinear piezoelectric dual sensor

In order to verify the algorithm, a pair of piezoelectric sensors with the structure shown in **Figure 15a** was fabricated and the sensing performance against the bending strain was evaluated. The bending deformation generated the voltage peak sign of each channel and this value was analyzed based on the linear equation on **Figure 14**. From there, the information of the bending radius and angle was derived. The real photographs for bending deformation 1, 2, and 3 that were applied to the test and the voltage peak values measured on each channel are shown in **Figure 15b**. The interpretation results were summarized in **Table 5**. We could confirm that the results obtained from the interpretation and the predictions of the radius and angle of the bend predicted from the photograph almost agree with each other. With this result, the capability of our algorithm based on the pair of piezoelectric sensors in simultaneously detecting the bending radius and angle was proved.

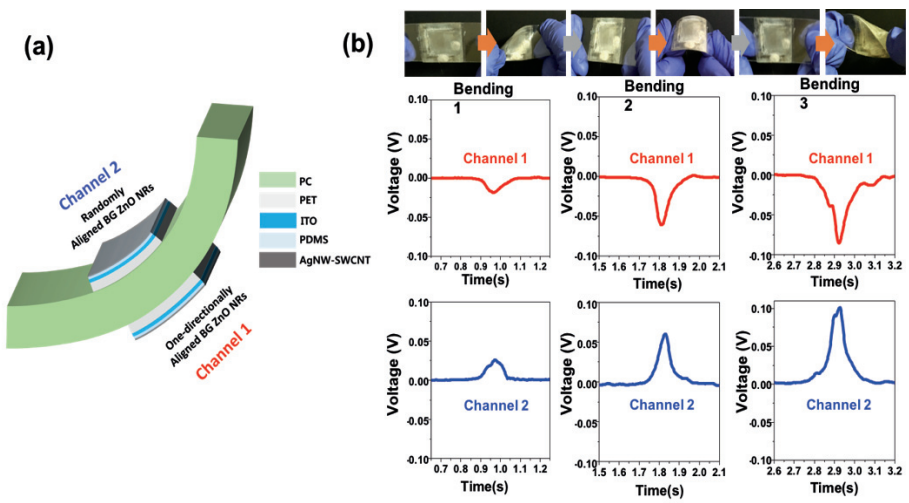

Figure 15. (a) Schematic diagram of nonlinear piezoelectric dual sensors (b) output voltage peaks from two channels under the three types of bending deformation.

Motion	Bending Radius (mm)	Bending Angle (°)
Bending 1	53.8	32.3
Bending 2	45.1	3.0
Bending 3	32.3	26.0

Table 5. Interpreted results for three kinds of bending deformations by using an algorithm proposed in this study.

Chapter 4. Conclusion

In conclusion, to detect various information of a bending deformation, we designed a sensor composed of a pair of nonlinear piezoelectric device based on BG-ZnO NRs, which could identify the bending angle as well as the bending radius. We fabricated the device based on the μ_{31} mode of BG-ZnO NRs with nonlinear piezoelectricity while taking the nonlinearity of the bending deformation and the convenience of the device fabrication process into consideration. Based on the anisotropic shape of one-dimensional nanomaterial BG-ZnO NRs, we constructed a one-directionally and randomly aligned device using the dry rubbing process with quantified the degree of alignment for each device. The voltage peak characteristics were measured according to the radius and angle of bending of each device with random and one-directional alignment. The results show that the randomly aligned device had no dependency on the bending angle and the one-directionally aligned device show a sensitive voltage peak change in the bending angle. This result was further confirmed through theoretical calculation using COMSOL Multiphysics®.

By using the characteristics of these two types of devices, a sensor capable of quantitatively sensing the radius and angle of the bending simultaneously was designed to integrate into a pair of the devices on the upper and lower surfaces of a substrate where bending deformation occurs. In addition, an algorithm was proposed as a sensing strategy, where a randomly aligned device first detected the bending radius and then based on this result, the bending angle was recognized by analyzing the voltage peak from the one-directionally aligned device. In order to verify the performance of the algorithm based on the sensor proposed in this study, a sensor composed of a pair of a randomly aligned device and a one-directionally aligned device was fabricated. The voltage peaks generated under various bending deformation were analyzed by the proposed algorithm, which successfully identified the radius and angle for each bending deformation.

In order for a sensor to detect bending deformation and for it to be applicable in the IoT technology, the information of the bending deformation should be more diverse. This study was worthy of consideration in that it proposes a unique device design and algorithm, which could simultaneously recognize the bending radius and angle beyond the limits of conventional bending sensors, which only recognizes the bending radius. It was expected that more similar research attempts will surface in the field of bending sensor research.

References

[1] D. –H. Kim, N. Lu, R. Ma, Y. –S. Kim, R. –H. Kim, S. Wang, J. Wu, S. M. Won, H. Tao, A. Islam, K. J. Yu, T. Kim, R. Chowdhury, M. Ying, L. Xu, M. Li, H. –J. Chung, H. Keum, M. McCormick, P. Liu, Y. –W. Zhang, F. G. Omenetto, Y. Huang , T. Coleman, J. A. Rogers, Science 333 (2011) 838-843.

[2] S Lee, A Reuveny, J Reeder, S Lee, H Jin, Q Liu, Nature Nanotechnology 11 (2016) 472-478.

[3] X Wang, B Yang, J Liu, C Yang J. Mater. Chem. A (2017), 5, 1176.

[4] AV Alaferdov, R Savu, TA Rackauskas, Nanotechnology 27 (2016) 375501.

[5] H He, Y Fu, W Zang, Q Wang, L Xing, Y Zhang, X Xue, Nano Energy 31 (2017) 37-48.

[6] D.H. Kim, Science 333 (2011) 1703–1703.

[7] C Majidi - Soft Robotics, (2014) 1(1):5-11.

[8] M Amjadi, A Pichitpajongkit, S Lee, S Ryu, I Park, ACS Nano(2014) 8 (5), pp5154–5163.

[9] Y. Cheng, R. Wang, J. Sun, L. Gao, Adv. Mater. 27 (2015) 7365-7371.

[10] L. Cai, L. Song, P. Luan, Q. Zhang, N. Zhang, Q. Gao, D. Zhao, X. Zhang, M. Tu, F.Yang, W. Zhou, Q. Fan, J. Luo, W. Zhou, P. M. Ajayan, S. Xie, Sci. Rep. 3 (2013) 3048.

[11] J. –S. Heo, J. –H. Chung, J. –J. Lee, Sens. Actuators A 126 (2006) 312-327.

[12] BJ Hansen, Y Liu, R Yang, ZL Wang, ACS nano, (2010) 4 (7) pp 3647–3652.

[13] M. Choi et al. Nano Energy 33 (2017) 462–468.

[14] M Lee, CY Chen, S Wang, SN Cha, YJ Park. Adv. Mater. (2012) 24, 1759–1764.

[15] S Rajala, T Siponkoski, E Sarlin, ACS Appl. Mater. Interfaces (2016) 8, 15607−15614.

[16] Q. Zheng et al, Nano Energy 26 (2016) 504–512.

[17] W. He et al, Applied Surface Science 392 (2017) 1055–1061.

[18] R. Yang, Y. Qin, L. Dai, Z. L. Wang, Nat. Nanotechnol (2009) 4, 34.

[19] N.R. Alluri et al, Composites Science and Technology 142 (2017) 65e78.

[20] S.K. Kim et al, Nano Energy 22 (2016) 483–489.

[21] Y.K. Fuh, B.S. Wang, Nano Energy 30 (2016) 677–683.

[22] W. S. Jang, T. I. Lee, J. Y. Oh, S. H. Hwang, S. W. Shon, D. H. Kim, Y. Xia, J. M.Myoung, H. K. Baik, J. Mater. Chem. 22 (2012) 20719-20727.

[23] Z Z Shao, L Y Wen, D M Wu, X F Wang, X A Zhang and S L Cha ng, J. Phys. D:Appl. Phys. 43 (2010) 245403.

[24] X Jiang, W Huang, S Zhang, Nano Energy (2013) 2, 1079–1092.

[25] A Chortos, J Liu, Z. Bao, Nature materials 15, (2016) 937-950.

[26] W. S. Jang, T. I. Lee, J. Y. Oh, S. H. Hwang, S. W. Shon, D. H. Kim, Y. Xia, J. M. Myoung, H. K. Baik, J. Mater. Chem. 22 (2012) 20719-20727.

요 약 (국문 초록)

Internet of things (IOT) 기술시대가 도래하면서 사물의 미세 한 움직임을 인지하는 센서에 대한 관심이 많이 높아지고 있는 가운데, 인공적인 센서 중 구부림을 인지하는 전자장치에 대한 연구가 활발히 진행되고 있다. 그 중에서도 압전재료를 기반으로 하는 센서는 외부 전원 장치가 필요 없고, 쉽게 제작할 수 있다는 측면에서, 주목을 받고 있다. 압전 구부림 센서에서의 구부림은 비선형적인 변형으로, 대부분의 압전 구부림 센서가 선형적인 압전상수인 d_{33}, d_{31}모드이며, 수직적 혹은 수평적으로 발생되는 전기적인 분극을 유도한다. 전기적인 분극의 방향은 in-plane 방향이나 out-plane방향으로 구분될 수 있고, 센서의 공정편이를 위해서는 out-of-plane으로의 연구가 많이 진행되고 있다. 이러한 배경으로 인해 비선형적인 압전모드에서, 구부림의 비선형적 변형의 압전센서에 대한 연구가 필요 하며, 진보적인 센서 기술을 위해서 다양한 구부림의 정보를 인지 할 수 있어야 한다.

본 연구는 압전재료 중 하나인 양쪽으로 성장한 산화아연을 한쪽 방향으로 정렬시켜서 구부림 곡률과 구부림 방향을 동시 인지할 수 있는 센서를 개발 하였다. 일반적인 압전재료와는 달리, 양쪽 방향으로 성장한 산화아연은 비선형 압전성의 변전상수인 u_{31}모드로 활성화되며,

구부림 변형에 적합한 비선형적인 압전 특징을 나타낸다. 이러한 비선형 압전특성을 장치를 개발함으로써 실험적으로 증명했고, COMSOL Multiphysics, 유한 요소법을 이용한 시뮬레이션 소프트웨어를 이용해 이론적인 계산을 통한 이론적인 부분과 실험적인 부분의 일치하는 메커니즘을 증명했다. 마지막으로 구부림곡률과 구부림방향을 동시적으로 인지하는 장치를 제조함으로써 실제로 다양한 구부림 변형을 가해주고, 발생 하는 전기적인 신호를 통해 인지가 가능하다는 것을 보였다.

주요어: 자가발전센서, 양쪽 성장 산화아연 나노로드, 비선형 압전성, 센싱알고리즘, 구부림 곡률, 구부림 각도

학번: 2015-26093